Chapter 12

Soil-plant cycle of silicon in basaltic ash soils under intensive banana cropping using δ^{30}Si and Ge/Si *

Abstract

In soils, silicon released by mineral weathering can be retrieved from soil solution through clay formation, Si adsorption onto secondary oxides, and plant uptake. These processes impact the Si isotopic signature and Ge/Si ratio of dissolved Si exported to rivers. Here we use these proxies to study the input of biogenic Si in a soil-plant system involving basaltic ash soils under intensive banana cropping. The soils strongly differed in weathering stage, from poorly developed (PD) to strongly weathered (SW) volcanic soils (vs). The values of δ^{30}Si and Ge/Si were determined in various compartments of the system: δ^{30}Si by MC-ICP-MS Nu Plasma in medium resolution, operating in dry plasma with Mg doping (δ^{30}Si vs NBS28 $\pm$ 0.12‰$\pm 2\sigma_{SD}$), Ge/Si computed after determination of Ge by HR-ICP-MS and Si by ICP-AES. Compared to fresh ash (δ^{30}Si = -0.38‰; Ge/Si = 2.21μmol/mol), soil clay fractions were enriched in light Si isotopes and Ge: with increasing weathering stage and clay content from PDvs to SWvs, δ^{30}Si (‰) decreased from -1.19 to -2.37, and Ge/Si (μmol/mol) increased from 4.10 to 5.25. Sand and silt fractions displayed δ^{30}Si close to fresh ash (-0.33‰) or higher (+0.18‰) due

*Article in preparation: Opfergelt et al.
Supplementary material in Appendix G

to saharian dust quartz contribution. Si isotopic signatures of bulk soils were strongly governed by the relative proportions of primary and secondary minerals. This strong control allows evaluating the dust quartz and biogenic Si (BSi) contributions in soil surface horizons. δ^{30}Si and Ge/Si signatures of clays support the occurence of a BSi source for Si sequestration in clays of PDvs surface horizons. δ^{30}Si and Ge/Si are thus highly pertinent proxies to study the Si soil-plant cycle, and to identify the major processes impacting the bulk soil isotopic signature. We conclude that both weathering and Si biocycling significantly impact the Si isotopic signature of pore waters.

12.1 Introduction

The global cycle of silicon is coupled to the carbon cycle through silicate weathering and CO_2 oceanic fixation by biota requiring essential Si (Raven and Edwards, 2001; Smetacek, 1999). By taking up Si, plants imprint the continental Si cycle (Alexandre et al., 1997; Derry et al., 2005; Lucas, 2001) and generate a biogenic Si (BSi) pool in soils (Blecker et al., 2006; Sommer et al., 2006), which in turn largely contributes to the hydrological ouput of Si (Derry et al., 2005). Taken up as aqueous monosilicic acid (Raven, 1983), Si is carried from roots to transpiration sites and precipitates as biogenic opal called phytoliths (Jones and Handreck, 1965). Plant species widely differ in Si content (Hodson et al., 2005). BSi returns to soil through falling litter and decomposition of plant debris, and yields up significant Si input to soil (Alexandre et al., 1997; Lucas et al., 1993). Soil BSi is rapidly recycled, particularly in the humid tropics (Alexandre et al., 1994 1997; Cary et al., 2005). The Si soil-plant feedback thus constitutes a separate cycle of major importance within the global Si cycle since BSi minerals are generally more soluble than other pedogenic and lithogenic silicates (Fraysse et al., 2006; Meunier, 2003). However, the relative proportion of weatherable lithogenic silicates and more stable, clay-sized, pedogenic minerals strongly governs the plant uptake of Si and thus the building-up of the BSi pool in the soil-plant system (Henriet, 2008).

Si stable isotopes and Ge/Si ratio (Derry et al. (2005); Ziegler et al. (2005a); Chapter 8) are promising tracers to study the Si soil-plant cycle in soils differing in weathering stage. Relative to crustal rocks, clay-sized weathering products are enriched in light Si isotopes (Ziegler et al., 2005ab) and Ge (Kurtz et al., 2002; Murnane and Stallard, 1990) through clay formation and Si and Ge adsorption onto Fe-oxide (Mortlock and Froelich (1987); Scribner et al. (2006); Chapter 10).

Plant uptake privileges light Si isotopes and Si against Ge in phytoliths, leading to a BSi pool depleted in heavy Si isotopes (Ding et al. (2005b 2008); Opfergelt et al. (2006b); Chapter 7) and Ge (Derry et al. (2005); Chapter 9). Consequently, dissolved Si (DSi) in rivers is enriched in heavy Si isotopes (Alleman et al., 2005; De La Rocha et al., 2000; Ding et al., 2004; Georg et al., 2006a 2007c).

Here, we study the Si cycle in a soil-plant system involving a Si-accumulating plant and a weathering sequence of soils derived from basaltic ash. The study was conducted to answer three questions: (1) How does weathering stage influence the bulk Si isotopic and Ge/Si signatures in soils? (2) How does BSi contribute to Si sequestration in soil clay-sized fractions through clay formation and Si adsorption onto Fe-oxide? (3) Are δ^{30}Si and Ge/Si relevant tracers of Si weathering and plant input in the Si soil-plant cycle involving a Si-accumulating plant? For these purposes, we selected soils derived from similar basaltic ash, but differing in weathering stage, under ancient intensive banana cropping. In humid tropical regions, soil weathering sequences in volcanic environments are remarkably suited to study the impact of weathering stage on soil properties (Chadwick et al., 2003; Delvaux et al., 1989) and soil BSi building-up (Henriet, 2008).

12.2 Materials and methods

12.2.1 Environmental setting

The study areas (Cameroon, West Africa) are located in : (1) the Mungo plain (60-350m asl; axis Njombé-Penja-Loum, 4°30'-4°53'N 9°37'-9°50'E, 70km north of Douala), (2) the low Eastern slopes of Mt Cameroon volcano (alt. 4095m) (400-900m asl; 4°09'-4°13'N 9°16'-9°21'E, 65 km west of Douala). They will be referred to as Mungo and Mt Cameroon (Figure 12.1). The climate is humid tropical with a rainy season extending from March to November and temperature ranging between 22.4°C (870m asl) and 27.5°C (40m asl) (Martin and Sieffermann, 1966). The average annual rainfall ranges between 2500 and 2800 mm year^{-1} in Mungo, and between 2250 and 2800 mm year^{-1} in Mt Cameroon.

The Mungo plain is a graben located between the stratovolcanoes Mt Cameroon and Mt Manengouba (Nkouathio et al., 2002), part of the N30°E Cameroon Hot Line (Déruelle et al., 2007). Mungo soils derive from basaltic ash and pumice deposits. Mt Cameroon soils develop from fine basaltic ash materials transported by mudflows. All materials are Quaternary in age: from early Quaternary era to present times. This age variation largely explains the contrasting weathering stages of

volcanic ash soils in this area (Delvaux et al., 1989; Sieffermann, 1973) and the weathering sequence Vitric Andosol - Andosol - Cambisol - Nitisol (classified according to ISSS (1998)).

Ancient banana cropping systems (since 1950's to present time) involve successive crop cycles of 6-9 months. At harvesting time, banana leaves and pseudostems are cut and left on soil surface. Banana fields are irrigated during the dry season by surrounding river waters; fertilizers (N, P, K, Mg) are applied on a monthly basis whereas lime is applied on a two-year basis.

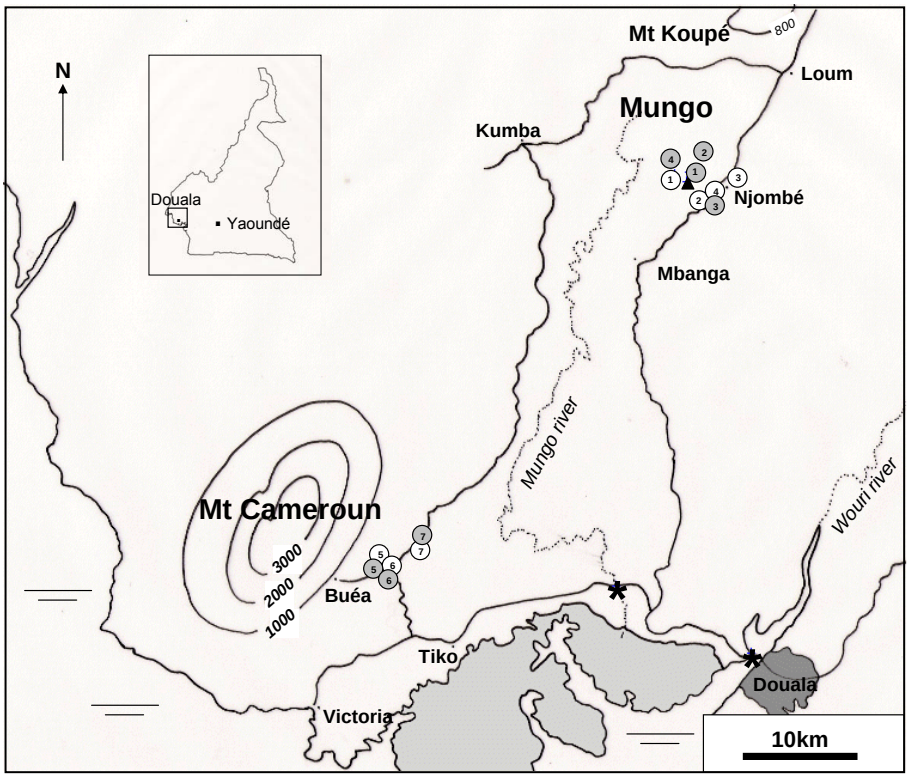

Figure 12.1: Location of sampling sites: soil profiles = grey number (1-Dia-Dia; 2-Sir; 3-Mbomé; 4-Djungo; 5-Molyko; 6-Ekona; 7-Mussaka) - irrigation station = white number (1-Dia-Dia lake; 2-Mbomé; 3-Koumbé; 4-Cofruca; 5-Mussaka; 6-MolykoA; 7-MolykoB) - rivers = stars - Mt Pelé = triangle. Light grey indicates mangroves.

12.2.2 Sampling

Sampling was realized in November 2005 at the end of the rainy season (sampling sites in Figure 12.1). Seven soil profiles were selected under ancient banana cropping systems. They cover a range of volcanic ash soils at different stages of weathering, from poorly developed (PD) to strongly weathered (SW) volcanic soils (vs). The selected Mungo soils (99-240 m asl) are, from PDvs to SWvs, Dia-Dia (DD), Sir (SR), Mbomé (MB) and Djungo (DJ). Mt Cameroon soils (545-685 m asl) are, from PDvs to SWvs, Molyko (MO), Ekona (EK) and Mussaka (MU).

Each soil profile was described according to FAO guidelines. Bulk samples were collected from each horizon. Two (PDvs) or three (SWvs) horizons were selected in each profile to cover surface and deeper horizons (cm): in Mungo, DD Ap 0-5, AC 5-40; SR Ap1 0-5, Bw 21-33; MB Ap 0-5, AC 5-40; DJ Ap1 0-5, Bt 15-66, Bw 66-115; in Mt Cameroon, MO Ap2 5-20, Bw1 20-60, Bw2 60-92; EK Ap2 5-32; Bt 32-60, Bw1 60-100; MU Ap2 5-25, Bt1 5-25, Bt2 65-110. Samples were air dried at room temperature during 24 h and sieved at 2mm (fine earth fraction FEF<2mm).

Quaternary basaltic pyroclasts in Mungo and Mt Cameroon share a common mineralogical composition as they both belong to the same *Upper black Serie* (Dumort, 1968). Fresh pumice was collected from the most recent volcanic cone in the Mungo plain (Mont Pelé). We also used soil samples from surface horizons from four Mungo soil profiles previously studied (Delvaux et al., 1989 1990b): MB2 Ap 0-12, SN4 Ap 0-20, SN2 Ap1 0-8, MK1 Ap 0-11 from from PDvs to SWvs.

Stream waters used for crop irrigation were sampled (Figure 12.1) at four locations in Mungo (Dia-Dia lake, Mbomé, Cofruca, Koumbé) and three in Mt Cameroon (Molyko A, Molyko B, Mussaka). River waters from Mungo river (Tiko) and Wouri river (Douala) were also collected (Figure 12.1). Water samples were immediately filtered through 0.45μm polycarbonate membranes, acidified with suprapur HNO_3 and stored at fresh temperature in the dark, in acid-cleaned polypropylene bottles. Filters were dried at 60°C.

12.2.3 Characterization of the samples

Physical, chemical and mineralogical characterization of the soil

The particle size distribution of FEF samples was determined by quantitative recovery of clay (<2μm), silt (2-50μm) and sand (>50μm) fractions after sonication and dispersion with Na^+-saturated resins

(Rouiller et al., 1972). Briefly, sand fractions were obtained through ultrasonic dispersion of FEF and repeated wet sieving. Clay and silt fractions were then collected and submitted to prolonged dispersion with Na^+-resins. Clay was separated from silt by successive cycles of 24h decanting and pipetting.

Elemental analysis of clay and FEF was carried out after loss on ignition at 950°C followed by borate fusion (Chao and Sanzolone, 1992). Briefly, a crushed sample of 100 mg was melted at 1000°C for 5 minutes in a graphite crucible in the presence of 0.4 g Li-tetraborate and 1.6 g Li-metaborate. The cooled melt was then dissolved in 100 ml of 2M HNO_3 under magnetic agitation at 90-100°C. Elemental contents were determined by ICP-AES. The total contents of alkaline and alkaline-earth cations were summed up as the total reserve in bases (TRB), which estimates the content of weatherable minerals in mineral soil horizons (Herbillon, 1986). Dark oxalate (o) and dithionite-citrate-bicarbonate (DCB) extractable contents of Si, Al, Fe were determined on fine earth and clay fractions by well-known extraction procedures (o: Blakemore et al. (1981); DCB: Mehra and Jackson (1960)), and determination by ICP-AES. Oxalate extraction is selective for allophanic constituents (amorphous) without dissolving opaline and crystalline silica (Wada, 1982).

The mineralogy of sand, silt and amorphous silica (ASi) fractions was determined by powder X-ray diffraction (XRD, Cu Kα, D8). Clay minerals were identified by XRD after K^+ and Mg^{2+} saturation, ethylene glycol (EG) solvation and thermal treatments at 300°C and 550°C (Robert and Tessier, 1974).

Phytoliths extraction from soil

Phytoliths were extracted from Mungo soil horizons by a heavy liquid method adapted from Kelly (1990). Amorphous Si (ASi) was recovered by this method, and includes silt-sized particles having a density below 2.3 $g.cm^{-3}$, i.e. phytoliths (plant biogenic Si: BSi), diatoms and volcanic glasses. Most phytoliths fall in the 5-200μm size range (Zhao and Pearsall, 1998), but they are particularly abundant in the 5-50μm fraction (Jones and Beavers, 1964) and less frequent in the fractions above 50μm (Herbauts et al., 1994). Here, the silt fraction (2-50μm) was treated by H_2O_2 30% until full oxidation of organic matter, and thereafter by DCB to extract iron oxides. A new cycle of dispersion with Na^+-resin followed by decanting and pipetting eliminated clay contamination. ASi was then recovered by densimetric separation with an heavy liquid $ZnBr_2$ (d=2.3 $g.cm^{-3}$). Each silt fraction was mixed with

20 cm^3 of $ZnBr_2$ and centrifuged at 4000t.min^{-1} for 10 minutes. The supernatant containing the floating phytoliths was carefully removed with a pipette and collected in a glass vessel through a Teflon (PTFE) filter (2μm) soaked with ethanol. Each silt fraction was mixed again with $ZnBr_2$, and the operation was repeated until the supernatant was clear. The filter was abundantly rinsed with 1M HCl and distilled water, and dried at 105°C for gravimetrical quantification. Residual silts were also cleaned with 1M HCl and distilled water and recovered for further characterization. Rapid screening by optical microscopy and XRD characterization of ASi fractions were realized, and total elemental content was measured by ICP-AES after alkaline fusion.

Silicon in river waters

Dissolved Si (DSi) content in river waters was determined by ICP-AES. Biogenic silica (BSi) content from suspended load in rivers was carefully dissolved by 0.2 M NaOH leaching at 100°C on the filters (Ragueneau et al., 2005) and measured by acid-molybdate colorimetric method (Strickland and Parsons, 1968). Contribution of clays (lithogenic Si, LSi) was corrected with Al concentrations measured by HR-ICP-MS with a detection limit of 0.01μM Al. Rapid screening of suspended load filtered was carried out by scanning electron microscopy (SEM) using a high resolution Digital Scanning microscope 982 Gemini from Leo operating at 1 kV.

12.2.4 Tracers of silicon

Silicon isotopes analyses

The Si isotopic composition was measured in (1) fresh basaltic pumice, (2), sand, silt, clay and ASi fractions as well as DCB-treated clays from Mungo, (3) clay fractions from Mt Cameroon, (4) oxalate extract from DD Ap (Mungo), (5) FEF samples of DD and DJ surface (Ap) horizons, (6) river waters. From rock/soil samples, silicon was recovered from each aliquot by alkaline fusion at 1000°C of 5mg of silicate powder mixed with 30mg of $LiBO_2$ flux in a covered Pt crucible and dissolution in double distilled 5% HNO_3 (Abraham et al. (2008); Chapter 5). Dissolved Si (rock/soil and river waters) was purified by triethylamine molybdate (TEA-moly) co-precipitation and combustion in covered Pt crucibles at 1000°C (De La Rocha et al., 1996), and dissolved in dilute suprapur HF-HCl mixture (Cardinal et al., 2003).

The Si-isotopic compositions (δ^{30}Si and δ^{29}Si) were measured using a Nu Plasma MC-ICP-MS operating in dry plasma mode, with an

external Mg doping to correct mass bias (Cardinal et al., 2003) and solving the isobaric interference of $^{14}N^{16}O$ on ^{30}Si (Abraham et al. (2008); Chapter 5). The analytical method was supported by an inter-laboratory comparison exercise and proved to be accurate on secondary reference materials (Reynolds et al. (2007); Chapter 6). Quality control of the measurements was given by reference materials (diatomite, BHVO) joined to each sample series, falling on the recommanded values (Reynolds et al. (2007); Chapter 6; Abraham et al. (2008); Chapter 5). To avoid matrix effects, absence of major elements and Mo was controlled by ICP-AES before MC-ICP-MS analyses. Data were obtained by the sample-standard bracketing technique relative to the NBS28 silica sand standard (National Institute of Standard and Technology RM #8546) for silicon isotopes or in house standards ($pSiO_2$ or Quartz Merck) isotopically similar to NBS28 (Abraham et al. (2008); Chapter 5). Our results were expressed as δ^{30}Si vs. NBS28 (‰) with an average precision and accuracy on total replicates of 0.12‰ ($\pm$ $2\sigma_{SD}$) following:

$$\delta^{30}Si = \left[\frac{\left(\frac{^{30}Si}{^{28}Si}\right)_{sample}}{\left(\frac{^{30}Si}{^{28}Si}\right)_{NBS28}} - 1 \right] \times 1000$$

Quality control of the mass fractionation is given by the δ^{29}Si vs. δ^{30}Si plot (Suppl. Mat., Figure G.1). Few data obtained as δ^{29}Si values were converted to δ^{30}Si values by using the multiplying factor 1.93 assuming a mass-dependent fractionation process (Young et al., 2002) following the equilibrium fractionation law. This is supported by equilibrium fractionation processes observed in natural rivers (Georg et al., 2006a 2007c).

Germanium/silicon ratio

Ge/Si ratio was computed from Ge and Si contents. The samples were dried at 105°C, dissolved by borate fusion (sample:$LiBO_2$ in 1:1 ratio) at 1000°C during 1 hour in platinum crucible. The dissolution of fusion beads was carried out in 5% HNO_3 solution. Ge was measured in the solution by HR-ICP-MS in medium resolution with In as internal standard and a reproductibility of 3.7%. The detection limit in solution (10.1μg l^{-1}) was determined by measuring 7 blanks. Si content was analysed by ICP-AES with Au and Y as internal standards and a reproductibility of 2.7%. The detection limit in solution (0.35 mg l^{-1}) was determined by measuring 6 blanks.

12.3 Results

12.3.1 Properties of soil and clay materials

Major characteristics of the fine earth and clay fractions of the selected soils are presented in Table 12.1 (see also Suppl. Mat. in Appendix G, Table G.1, G.2, G.3; Figure G.2, G.3). Weathering indexes (clay content, TRB, (Fe_d-Fe_o)/Fe_t ratio) give a good control on the relative weathering stage of the selected soils (Suppl. Mat., Figure G.3). They highlight the increased weathering stage from DD (Vitric Andosol) to SR, MB (Andosol) and DJ (Nitisol) in Mungo, and from MO (Andosol) to EK (Cambisol) and MU (Nitisol) in Mt Cameroon (nomenclature following ISSS (1998)). In each sequence, clay content increased and TRB (Suppl. Mat., Table G.2) decreased from PDvs to SWvs, in excellent agreement with previous data (Delvaux et al., 1989; Sieffermann, 1973). All weathering indexes indicate a more advanced weathering stage in Mt Cameroon soils compared to Mungo. Total Si content in FEF decreased from PDvs to SWvs (38.5-34.8 %SiO_2 in Mungo and 36.3-27.9 %SiO_2 in Mt Cameroon), supporting progressive desilication and relative concentration of less mobile Al and Fe (Suppl. Mat., Table G.1). The weathering sequence corresponds to the mineralogical sequence ash-allophane-halloysite-kaolinite (Delvaux et al., 1990b). Mungo Si_o data show that allophanic constituents became progressively dominant from DD to SR and MB and disappeared in DJ (Suppl. Mat., Table G.3). In Mt Cameroon, they occured in MO and EK and disappeared in MU (Suppl. Mat., Table G.3). The occurrence of allophane in these sequences is strongly correlated to the relative weathering stage of soil (Delfosse et al., 2005b), confirming the more advanced weathering stage of MO relative to DD (Suppl. Mat., Figure G.2).

12.3.2 Silicon distribution in the soil

Amorphous Si fraction extracted by heavy liquid

ASi contents (including BSi) ranged between 0.6 and 1.8% (Table 12.1). For comparison, soil BSi content ranges from 0.54 to 0.91% in other African soils (Runge, 1999) and from 0.20 to 0.26% in equatorial rainforest (Alexandre et al., 1994). The ASi content corresponds to a range of 6.0-17.7 $g.kg^{-1}$ calculated, falling in that of soil biogenic opal content (1-30 $g.kg^{-1}$; Drees et al. (1989)). SR and MB soils contain more ASi than DD and DJ, and DD presents the lowest ASi in both the surface and deep horizons. The Al/Si atomic ratio was below 0.02 in all ASi fractions, indicating a very low Al contamination of the ASi

Table 12.1: Particle size distribution (%): sand (>50μm), silt without ASi fraction (2-50μm), amorphous silica fraction extracted from silt by heavy liquid (ASi, 2-50μm), clay (<2μm); Total Reserve in Bases (TRB); Contents of total Si (Si_t), DCB-extractable Si (Si_d), and oxalate extractable Si (Si_o) in fine earth fraction (FEF<2mm) and clay fraction (<2μm).

Sample ID			Sand	Silt	ASi	Clay	Fine earth				Clay fraction			
Prof.	Horiz.	Depth cm	>50μm %	2-50μm %	2-50μm %	<2μm %	TRB $cmol_c.kg^{-1}$	Si_t	Si_d	Si_o	Si_t	Si_d	Si_o
								$g.kg^{-1}$				$g.kg^{-1}$		
DD	Ap	0-5	61	14	0.6	25	703	180	3.2	7.1	74	8.6	10.1
DD	AC	5-40	61	15	0.6	24	712	188	3.7	8.9	75	10.2	15.0
SR	Ap1	0-5	20	37	1.3	42	469	150	4.0	17.3	104	9.5	10.0
SR	Bw	21-33	16	40	1.2	43	526	170	4.1	21.9	108	11.8	38.8
MB	Ap	0-5	16	25	1.8	58	323	122	4.3	6.8	99	4.6	1.5
MB	AC	5-32	25	36	1.4	37	438	181	4.3	22.4	129	11.8	29.7
DJ	Ap1	0-5	10	17	0.8	72	183	163	3.9	2.8	140	5.4	2.2
DJ	Bt	15-66	6	10	0.9	84	126	176	3.8	2.6	158	6.1	1.9
DJ	Bw	66-115	9	5	1.5	85	84	193	3.8	2.0	167	5.5	1.8
MO	Ap2	5-20	20	31	-	49	468	170	3.8	15.9	131	7.6	0.5
MO	Bw1	20-60	22	27	-	51	408	161	5.0	22.3	127	7.6	0.5
MO	Bw2	60-92	35	26	-	39	604	151	3.9	33.6	130	8.0	0.7
EK	Ap2	5-32	11	31	-	59	273	158	4.9	16.3	151	9.0	0.6
EK	Bt	32-60	10	27	-	64	252	159	5.3	21.0	146	9.0	0.6
EK	Bw1	60-100	13	30	-	56	321	145	5.4	36.1	141	10.4	0.7
MU	Ap2	5-25	4	24	-	72	63	130	0.8	0.4	160	1.1	0.1
MU	Bt1	25-65	3	14	-	83	43	148	0.7	0.3	169	0.9	0.1
MU	Bt2	65-110	2	12	-	86	48	147	0.7	0.3	169	1.1	0.1

pool. XRD revealed that the ASi fraction was constituted by opal-A, detected by a diffused broad diffraction band centered at about 0.40nm (Suppl. Mat., Figure G.4) (Drees et al., 1989). Observations by optical microscopy revealed the presence of phytoliths in the ASi fraction of the Mungo surface horizons whereas no phytoliths were observed in deeper horizons (Suppl. Mat., Figure G.5).

Contribution of fractions to the total Si content of the soils

Contributions of the different fractions to the total Si content of FEF is presented in Figure 12.2 for Mungo. Primary minerals are concentrated in sand and silt fractions and largely contribute to Si content in DD, SR and MB. Sand fractions also include quartz, probably from saharian dust particles in surface horizons (Chauvel et al., 2002). The contribution of ASi to total Si (Si_t) was similar in all soil horizons. However, phytoliths (BSi) were only observed in surface horizons (Ap). Secondary silicates in the clay fraction can be subdivided into non-crystalline (Si_o) and crystalline minerals (Si_t-Si_o). The proportion of non-crystalline clays (allophanic constituents) is maximum in SR and MB. The proportion of crystalline clay minerals (halloysite, kaolinite) increases from DD to DJ with increasing weathering stage. This fraction dominantly contributes to the total Si content in DJ soil.

12.3.3 Silicon isotopic signatures of soil fractions

The isotopic signatures of soil fractions are presented in Table 12.2. In Mungo (Figure 12.3), primary minerals from sand and silt fractions displayed δ^{30}Si (-0.33‰) close to that of fresh basaltic pumice (-0.38‰), or more positive (+0.18‰). Untreated clays were significantly lighter (-0.90 to -2.95‰) than fresh pumice. This trend of decreasing δ^{30}Si was observed through the Mungo sequence from DD to SR, MB and DJ, and also from MO to EK and MU in Mt Cameroon (Table 12.2). This trend accords with isotopic data performed on soils previously studied (Delvaux et al., 1989) from MB2 to MK1 (Table 12.2). This trend is also highlighted by the difference between DD and DJ bulk soil signatures (δ^{30}Si = -0.41 and -1.41‰ respectively, Table 12.2). DCB-treated clays (Mungo) displayed generally heavier signatures than their corresponding untreated clays (Table 12.2; Figure 12.3), particularly in DJ (SWvs). ASi fractions displayed δ^{30}Si from -0.55 to +0.60‰ with a systematic trend of higher values in surface horizons Ap (Figure 12.3). At depth, the ASi signature was close to that of fresh pumice. The

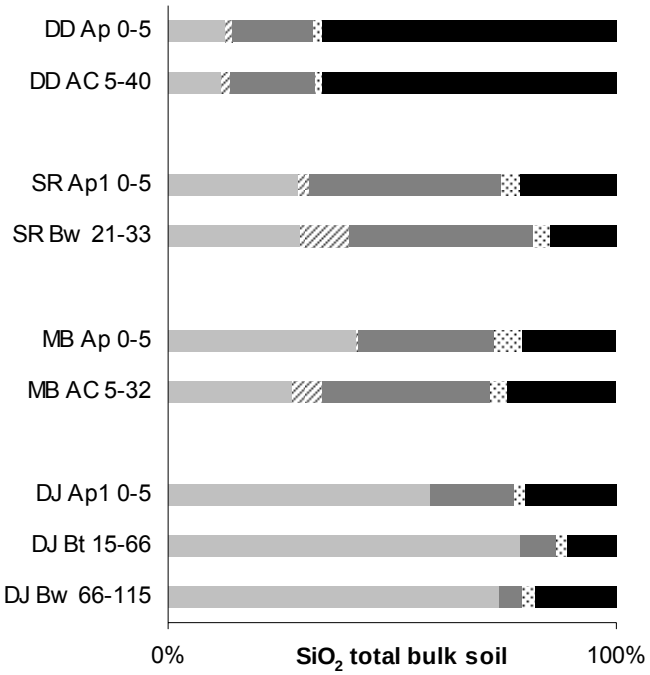

Figure 12.2: Contribution of the different fractions to total Si (100%) in the Mungo soils. Sand = black, ASi = dotted, silt = dark grey, non crystalline clay minerals (oxalate) = hatched, crystalline clay minerals = light grey.

oxalate-extractable fraction displayed a δ^{30}Si of -0.37‰, very close to the single value published so far for allophane (-0.4‰; Douthitt (1982)).

12.3.4 Germanium/silicon ratios in soils

The values of Ge/Si ratio are presented in Table 12.2. In Mungo, FEF samples of DD and DJ Ap horizons (0-5cm) displayed higher Ge/Si ratios than fresh pumice (2.21μmol/mol) did. Ge/Si was higher in the bulk soil (0-5cm) SWvs DJ (3.70 μmol/mol) than in the PDvs DD (2.50 μmol/mol). Relative to bulk soils, clays from DD and DJ surface horizons (Ap) were much more enriched in Ge (Ge/Si: 4.10-5.25 μmol/mol). In the SWvs DJ, Ge/Si values of clays (5.25-6.44 μmol/mol) were close to that of kaolinite (5.9 μmol/mol; Kurtz et al. (2002)). In Mt Cameroon, Ge/Si ratios of clays ranged between 3.13 and 5.04 μmol/mol.

Table 12.2: Isotopic signatures (δ^{30}Si vs. NBS28 ± st error $2\sigma_{SEM}$ (‰)) of the different soil fractions (sand, silt, ASi, clay (untreated), DCB-treated clay), fresh basaltic pumice, bulk soil (FEF) and oxalate extract (DD Ap); Ge/Si ratio (μmol/mol) in the clay fractions (untreated), bulk soil and fresh basaltic ash.

Prof.	Horiz.	Sand		Silt		ASi		Clay		DCB-clay		Clay
		δ^{30}Si	$2\sigma_{\mathrm{SEM}}$	δ^{30}Si	$2\sigma_{\mathrm{SEM}}$	δ^{30}Si	$2\sigma_{\mathrm{SEM}}$	δ^{30}Si	$2\sigma_{\mathrm{SEM}}$	δ^{30}Si	$2\sigma_{\mathrm{SEM}}$	Ge/Si
DD	Ap	**-0.33**	0.12	**-0.03**	0.13	**-0.38**	0.12	**-1.19**	0.12	**-1.10**	0.14	4.10
DD	AC	-	-	-	-	**-0.55**	0.13	**-1.52**	0.13	**-1.35**	0.12	5.27
SR	Ap1	**-0.28**	0.13	**-0.27**	0.14	**+0.15**	0.12	**-0.90**	0.13	**-1.24**	0.12	2.91
SR	Bw	-	-	-	-	**+0.01**	0.12	**-1.29**	0.13	**-1.21**	0.13	4.15
MB	Ap	**-0.06**	0.15	**+0.00**	0.12	**+0.60**	0.13	**-1.66**	0.14	**-1.05**	0.11	2.35
MB	AC	-	-	-	-	**-0.11**	0.17	**-2.07**	0.15	**-2.04**	0.15	4.45
DJ	Ap1	**+0.18**	0.15	**-0.44**	0.15	**+0.58**	0.14	**-2.37**	0.12	**-2.03**	0.14	5.25
DJ	Bt	-	-	-	-	**-0.29**	0.10	**-2.59**	0.16	**-2.14**	0.13	5.94
DJ	Bw	-	-	-	-	**-0.44**	0.11	**-2.12**^{b}	0.09^{c}	**-2.04**	0.14	6.44
MO	Ap2	-	-	-	-	-	-	**-2.93**	0.13	-	-	3.55
MO	Bw1	-	-	-	-	-	-	**-1.02**	0.12	-	-	3.13
MO	Bw2	-	-	-	-	-	-	**-2.95**	0.13	-	-	3.47
EK	Ap2	-	-	-	-	-	-	**-2.25**	0.13	-	-	5.04
EK	Bt	-	-	-	-	-	-	**-1.57**	0.13	-	-	4.42
EK	Bw1	-	-	-	-	-	-	**-2.23**	0.15	-	-	3.72
MU	Ap2	-	-	-	-	-	-	**-2.49**	0.12	-	-	3.91
MU	Bt1	-	-	-	-	-	-	**-1.54**	0.12	-	-	4.53
MU	Bt2	-	-	-	-	-	-	**-2.48**^{b}	0.16^{c}	-	-	4.32
MB2	Ap	-	-	-	-	-	-	**-1.15**^{a}	0.16	-	-	-
SN4	Ap	-	-	-	-	-	-	**-1.83**^{a}	0.15	-	-	-
SN2	Ap1	-	-	-	-	-	-	**-1.81**^{a}	0.14	-	-	-
MK1	Ap	-	-	-	-	-	-	**-1.77**^{a}	0.18	-	-	-

Sample		δ^{30}Si	$2\sigma_{\mathrm{SEM}}$	Ge/Si
Fresh basaltic pumice		**-0.38**$^{a.b}$	0.07^{c}	2.21
DD	Ap oxalate	**-0.37**	0.12	-
DD	Ap (0-5cm) bulk soil (FEF)	**-0.41**$^{a.b}$	0.30^{c}	2.50
DJ	Ap1 (0-5cm) bulk soil (FEF)	**-1.41**$^{a.b}$	0.18^{c}	3.70

^{a} δ^{30}Si calculated from δ^{29}Si with 1.93 factor, ^{b} mean between two measurements, ^{c} standard deviation ($2\sigma_{\mathrm{SD}}$)

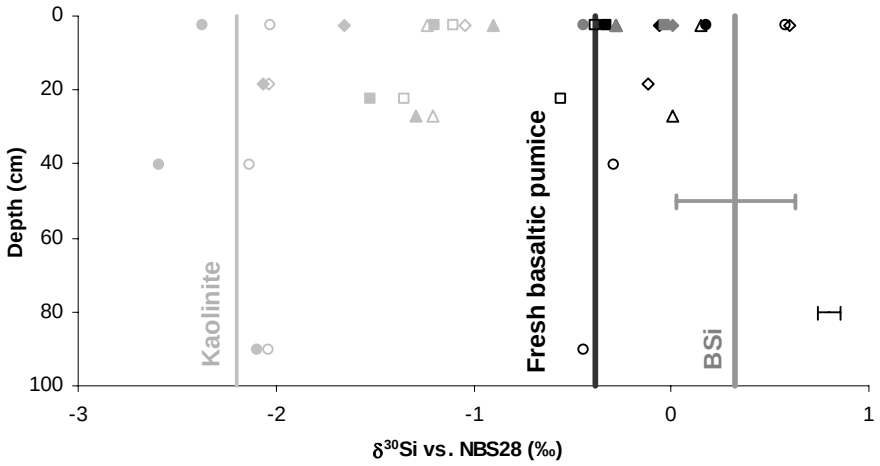

Figure 12.3: Isotopic characterization of soil fractions in the Mungo soils: sand = full black symbol, silt = dark grey symbol, clay (untreated) = full light grey symbol, DCB-treated clay = open light grey symbol, ASi = open black symbol. DD = square, SR = triangle, MB = diamond, DJ = circle. Kaolinite (Ziegler et al., 2005b) = light grey line, Fresh basaltic pumice = black line, Banana plant phytolith = dark grey line with grey error bar (Chapter 8). Black bracket shows the average standard deviation of full replicates ($\pm$ $2\sigma_{SD}$).

12.3.5 Silicon in river waters

Si content and Si isotopic signatures of river waters are presented in Table 12.3. Dissolved silicon content (DSi) in irrigation waters ranged between 306 and 989μM and is generally lower in rivers (231-324μMDSi). Our riverine DSi concentrations were above the ones measured in other Cameroon rivers (120-346μMDSi in Nyong, Viers et al. (2000); 141-174μMDSi in Nyong, Cary et al. (2005); 41-186μMDSi in Nsimi, Braun et al. (2005)), which could be attributed to the very rich Si-pyroclastic soils surrounding watersheds. Biogenic silica (BSi) content in suspended load varied between 0.23 and 3.40μMBSi, i.e. in the range of reported values from Cameroon (1.07 to 2.85μMBSi; Cary et al. (2005)). LSi varied between 0.35 and 6.53μMLSi, and BSi represented 26 to 71% of the total Si in suspended load. SEM observations on suspended load (including LSi and BSi) revealed that BSi was essentially constituted by diatoms (Suppl. Mat., Figure G.6). Phytoliths were expected as they were shown to largely contribute to particulate charge in Cameroon rivers (Cary et al., 2005). Small pieces of phytoliths can not be excluded

as observations were made without extracting LSi. However, no entire phytolith particles were observed.

The δ^{30}Si values of the DSi pool of irrigation waters at Dia-Dia lake, Mbomé, Cofruca and Koumbé pumping stations ranged between +0.99 and +1.35‰. River waters displayed δ^{30}Si at +1.01‰ (Wouri) and +0.91‰ (Mungo). The mean δ^{30}Si value for irrigation waters (+1.19 ± 0.07‰) was in the range of other published data for rivers (+0.4 to +1.2‰, De La Rocha et al. (2000); +0.7 to +3.4‰, Ding et al. (2004); +0.7 to +2.5‰ Alleman et al. (2005); +0.84 ± 0.19‰, Georg et al. (2006a); -0.08 to +1.46‰, Georg et al. (2007c)).

Table 12.3: Characterization of Si in stream waters used for crop irrigation (Mungo, Mt Cameroon) and in two Cameroon rivers (Wouri, Mungo): dissolved Si (DSi) content, biogenic Si (BSi) and lithogenic Si (LSi) content in suspended load, and fraction of BSi in the total Si of the suspended matter (%Si tot_{SPM}), isotopic signature (δ^{30}Si vs.NBS28) of DSi.

Zone	Station	DSi μM Si	BSi μM Si	LSi μM Si	BSi % Si tot_{SPM}	$\delta^{30}Si_{DSi}$ * ‰
Mungo	Dia-Dia	306	1.39	0.58	71	+1.35
	Mbomé	915	1.33	0.73	65	+1.14
	Koumbé	896	2.99	6.53	31	+1.26
	Cofruca	989	0.23	0.65	26	+0.99
Mt Cameroun	Mussaka	595	3.40	2.34	59	-
	Molyko A	698	0.95	1.13	46	-
	Molyko B	687	0.74	0.35	68	-
Rivers	Wouri	231	-	-	-	+1.01
	Mungo	324	-	-	-	+0.91

* calculated from δ^{29}Si with 1.93 factor

12.4 Discussion

12.4.1 Si tracers and soil weathering stage

Figure 12.4 illustrates the inverse relationship between δ^{30}Si and Ge/Si. With increasing weathering stage, δ^{30}Si decreases whereas Ge/Si increases. From fresh pumice (basaltic parent material) to the most weathered and clayey DJ soil, clays from Mungo soils progressively become enriched in light Si isotopes and Ge. Their isotopic and geochemical signatures evolve close to the ones of kaolinite (Figure 12.4a). For Mt Cameroon, the trend is less clear, but both δ^{30}Si and Ge/Si range between those measured for the fresh pumice and kaolinite (Figure 12.4b). The overall trend means that (i) clay minerals preferentially incorporate light Si isotopes (Ziegler et al., 2005b), (ii)

Ge is incorporated into secondary weathering products (Kurtz et al., 2002; Murnane and Stallard, 1990). Weathered soils are enriched in Fe-oxides. Consequently, sequestration of light Si isotopes and Ge by clay-sized Fe-oxides can not be excluded (Scribner et al. (2006); Chapter 10; Chapter 11). The adsorbed Si and Ge pools can not be represented in Figure 12.4 since we do not have any control on Ge/Si fractionation induced by adsorption onto Fe-oxides in these soils. Yet, this could explain the discrepancy between the two weathering sequences since Si isotopic fractionation caused by Si adsorption depends on both the Fe-oxide content and type (Chapter 11).

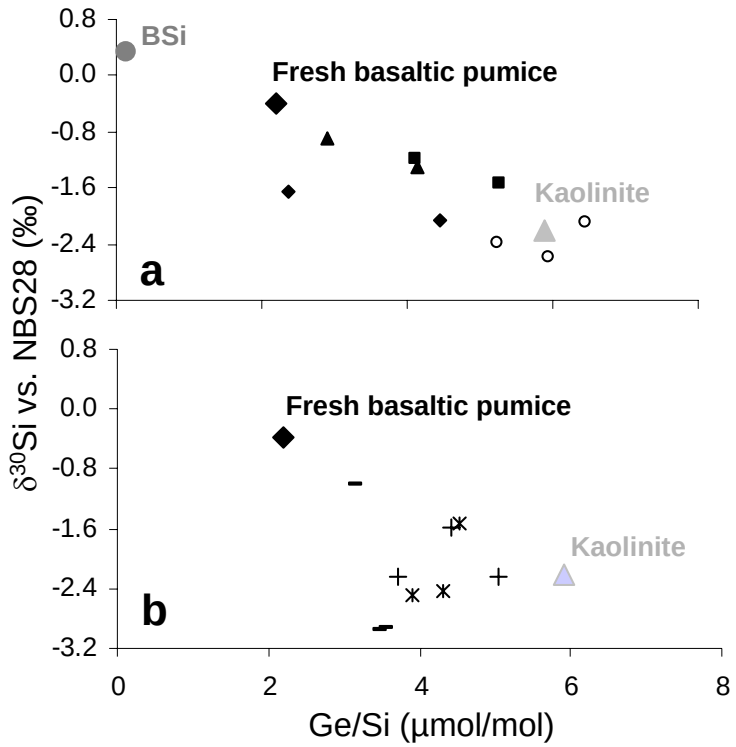

Figure 12.4: Plot of δ^{30}Si vs. Ge/Si in clay fractions of both weathering sequences. (a) Mungo: DD = square, SR = triangle, MB = diamond, DJ = open circle. (b) Mt Cameroon: MO = dash, EK = cross, MU = star. Main reservoirs: Fresh basaltic pumice = large black diamond, Kaolinite = large light grey triangle (Ziegler et al., 2005b), Banana phytoliths = large dark grey circle (Chapter 8; Chapter 9).

12.4.2 Silicon isotopic balance in the soil

Contribution of saharian dust to sand fraction

The Si isotopic signature of fresh basaltic pumice (-0.38‰) is consistent with the isotopic composition published for basalt (-0.31‰, Abraham et al. (2008); Chapter 5; -0.30‰, Georg et al. (2007b)). Sand fractions rich in primary minerals should display a signature close to that (-0.38‰). However, sands from DJ (+0.18‰), and to a lesser extent from MB (-0.06 ‰), revealed heavier signatures. This indicates an external Si source. Surface horizons (Ap) are exposed to saharian dust in this area (Chauvel et al., 2002). The presence of quartz was identified by XRD. Quartz displays heavier isotopic composition (Rose Quartz Standard = -0.02‰; Georg et al. (2007b)). Assuming that sand fraction is constituted of primary minerals (-0.38‰) and quartz (-0.02‰), the proportion of SiO_2 from quartz in sand fraction can be calculated from the Si isotopic signature of the total sand fraction (Table 12.4). Assuming 100% of SiO_2 in quartz and taking into account the measured SiO_2 content of the sand fraction, the quartz % in the sand fraction can be calculated. Taking into account the sand % in the soil, the quartz % in the soil can be evaluated (Table 12.4). The calculated quartz contents in Ap horizons of DD, SR, MB, DJ were 3, 2, 5 and 8%, respectively. This is very consistent with the quartz content (10%) reported in soils surrounding Mt Cameroon (Chauvel et al., 2002).

Crystalline clay minerals

The isotopic signature of crystalline clay minerals can be estimated by subtracting the contribution of allophanic constituents from the total Si content of clays, using Si_t and Si_o contents in clays (Table 12.1) and the proposed isotopic signature of allophane (-0.40‰; Douthitt (1982)). Figure 12.5a shows that crystalline clay minerals in SWvs display $\delta^{30}Si$ very close to that of kaolinite (-2.2‰, Ziegler et al. (2005b)). The abundance of kaolinite in SWvs was confirmed by XRD. The enrichment of light isotopes in secondary 1:1 clay minerals with weathering (Table 12.2, Figure 12.5a) accords with previous results reported by Ziegler et al. (2005a) in basalt weathering profiles.

Silicon adsorbed onto iron oxides

DCB-treated clays display heavier Si isotopic signatures compared to their untreated counterparts (Table 12.2). The DCB-extractable Si pool include Si adsorbed onto Fe-oxide surfaces (Chapter 10). Assuming that

Table 12.4: Isotopic balance calculation to evaluate (see details of calculation in section 12.4.2): (i) quartz content, (ii) δ^{30}Si of Si DCB-extracted, (iii) phytolith (BSi) content, (iv) bulk soil δ^{30}Si balanced by all the solid Si pools.

Quartz content calculation

Horizon	δ^{30}Si sand[a]	δ^{30}Si quartz[b]	δ^{30}Si prim.min.[a]	SiO_2 Qz/sand	Quartz[b]	Sand fraction[a]	%qz/sand	%sand/soil[a]	%qz/soil
	‰	‰	‰	proportion	SiO_2 %	SiO_2 %			
DD Ap	-0.33	-0.02	-0.38	0.14	100	33.2	0.05	61	3
SR Ap1	-0.28	-0.02	-0.38	0.28	100	35.3	0.10	20	2
MB Ap	-0.06	-0.02	-0.38	0.88	100	39.7	0.35	16	5
DJ Ap1	+0.18	-0.02	-0.38	1.00[c]	100	73.1	0.73	10	8

Si isotopic signature of Si DCB-extracted calculation

Horizon	δ^{30}Si clay[a]	δ^{30}Si DCB-clay[a]	Si_t clay[a]	Si_d clay[a]	Si DCB	Si clay	$\delta^{30}Si_{DCB}$	Mean $^{30}\varepsilon$[d]	$\delta^{30}Si_{source}$
	‰	‰	$g.kg^{-1}$	$g.kg^{-1}$	proportion	proportion	‰	‰	‰
DD Ap	-1.19	-1.10	74	8.6	0.12	0.88	-1.90	-1.16	-0.74
DD AC	-1.52	-1.35	75	10.2	0.14	0.86	-2.61	-1.10	-1.51
SR Ap1	-0.90	-1.24	104	9.5	0.09	0.91	-	-1.14	-
SR Bw	-1.29	-1.21	108	11.8	0.11	0.89	-1.98	-1.10	-0.88
MB Ap	-1.66	-1.05	99	4.6	0.05	0.95	-	-1.35	-
MB AC	-2.07	-2.04	129	11.8	0.09	0.91	-2.38	-1.19	-1.18
DJ Ap1	-2.37	-2.03	140	5.4	0.04	0.96	-	-1.45	-
DJ Bt	-2.59	-2.14	158	6.1	0.04	0.96	-	-1.45	-
DJ Bw	-2.12	-2.04	167	5.5	0.03	0.97	-	-1.47	-

Phytolith content calculation (BSi)

Horizon	δ^{30}Si ASi[a]	δ^{30}Si phyto[b]	δ^{30}Si glass[b]	SiO_2 phyto/ASi	BSi[b]	ASi fraction[a]	%phyto/ASi	%ASi/soil[a]	%phyto/soil
	‰	‰	‰	proportion	SiO_2 %	SiO_2 %			
DD Ap	-0.38	+0.11	-0.38	0.00	100	92.3	0.0	0.6	0.00
DD AC	-0.55	+0.11	-0.38	0.00	100	96.0	0.0	0.6	0.00
SR Ap1	+0.15	+0.33	-0.38	0.75	100	97.3	0.7	1.3	0.95
SR Bw	+0.01	+0.33	-0.38	0.55	100	97.3	0.5	1.2	0.63
MB Ap	+0.60	+0.33	-0.38	1.00[c]	100	97.0	1.0	1.8	1.72
MB AC	-0.11	+0.33	-0.38	0.38	100	96.9	0.4	1.4	0.51
DJ Ap1	+0.58	+0.54	-0.38	1.00[c]	100	97.4	1.0	0.8	0.82
DJ Bt	-0.29	+0.54	-0.38	0.10	100	96.0	0.1	0.9	0.09
DJ Bw	-0.44	+0.54	-0.38	0.00	100	92.2	0.0	1.5	0.00

End of table at the following page

[a] measured (see results): prim. min. = primary minerals, Si_t = total Si content of the clay fraction, Si_d = Si extracted by DCB from the clay fraction, ASi = amorphous Si fraction

[b] fixed (see text)

[c] these values were over 1 due to the $2\sigma_{SEM}$ error on the measured δ^{30}Si values. For calculation, they were fixed at 1.

[d] calculated from $^{30}\varepsilon$ of synthetic iron oxides and proportion of iron oxides in soils (see text)

Bulk soil Si isotopic signature calculation

Horizon	Sand fraction				Silt fraction			
	%sand/soil[a]	SiO_2%[a]	%SiO_2/soil proportion	δ^{30}Si ‰	%silt/soil[a]	SiO_2%[a]	%SiO_2/soil proportion	δ^{30}Si ‰
DD Ap	61	33.2	0.52	-0.33	14	40.6	0.14	-0.03
SR Ap1	20	35.3	0.21	-0.28	37	36.6	0.43	-0.27
MB Ap	16	39.7	0.24	-0.06	25	36.0	0.34	0.00
DJ Ap1	10	73.1	0.22	+0.18	17	40.8	0.20	-0.44

Horizon	ASi fraction				Clay fraction			
	%Asi/soil[a]	SiO_2%[a]	%SiO_2/soil proportion	δ^{30}Si ‰	%clay/soil[a]	SiO_2%[a]	%SiO_2/soil proportion	δ^{30}Si ‰
DD Ap	0.6	93.0	0.01	-0.38	25	15.8	0.10	-1.19
SR Ap1	1.3	97.9	0.04	+0.15	42	22.3	0.29	-0.90
MB Ap	1.8	97.6	0.07	+0.60	58	21.2	0.47	-1.66
DJ Ap1	0.8	97.9	0.02	+0.58	72	30.1	0.62	-2.37

Horizon	Soil**	δ^{30}Si soil	
	SiO_2%[a]	calculated	measured
DD Ap	38.5	-0.30	-0.41*
SR Ap1	32.2	-0.43	-
MB Ap	26.0	-0.76	-
DJ Ap1	34.9	-1.51	-1.41*

[a] measured (see results)

* calculated from measured δ^{29}Si with 1.93

** Total SiO_2 content of the soil horizon used to calculate the proportion of each fraction to the SiO_2 of the bulk soil

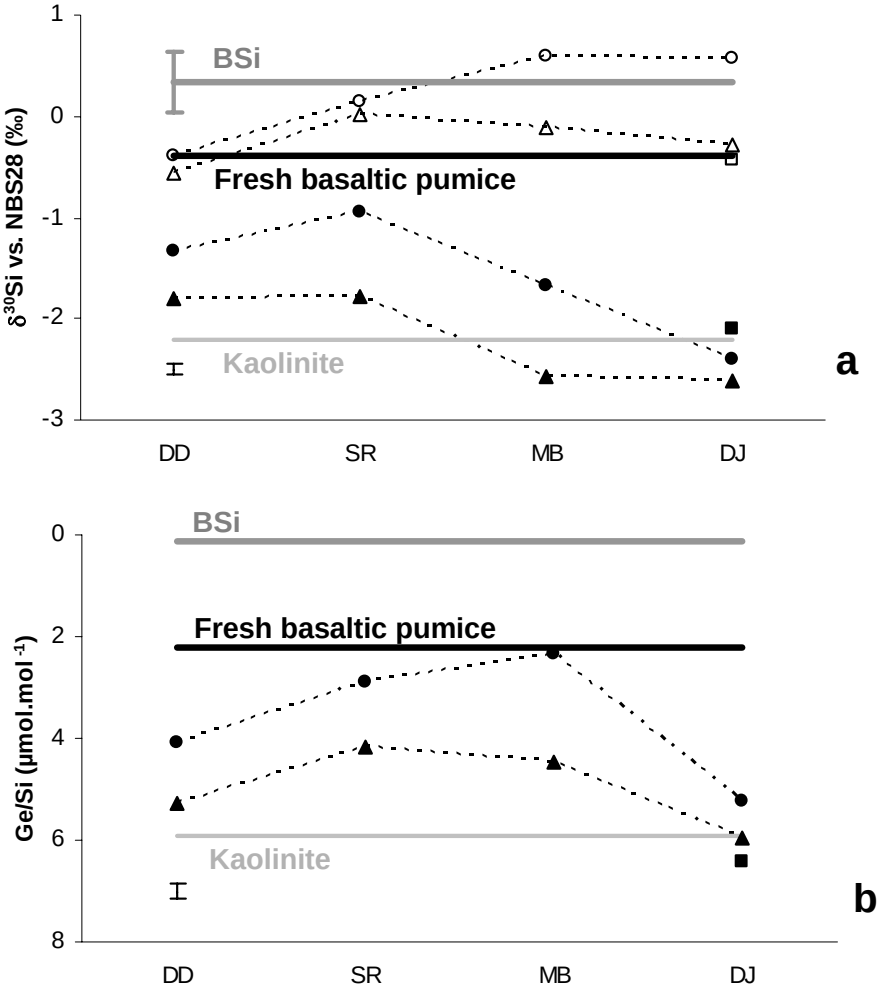

Figure 12.5: δ^{30}Si and Ge/Si values in Mungo soils: (a) Si isotopic signatures of (i) crystalline clays (full symbols), as calculated by subtracting clay-Si$_o$ from clay-Si$_t$, and using allophane δ^{30}Si (see section 12.4.2), and (ii) ASi fractions (open symbols); (b) Ge/Si ratios of clay fractions (untreated). Surface horizon (Ap) = circle, below surface horizon (AC, B) = triangle, deep horizon (B) = square. Main reservoirs: Fresh basaltic pumice = black line, Banana phytoliths = dark grey line (δ^{30}Si with grey error bar, Chapter 8; Ge/Si, Chapter 9), Kaolinite = light grey line (δ^{30}Si, Ziegler et al. (2005b); Ge/Si, Kurtz et al. (2002)). Black bracket shows the average standard deviation of full replicates ($\pm$ 2σ_{SD}).

$\delta^{30}Si_{clay}$ = [$\delta^{30}Si_{clayDCB}$ * proportion of Si from clay-DCB] + [$\delta^{30}Si_{DCB}$ * proportion of Si from Si-DCB], and taking into account the proportion of Si DCB (Si_d) in the total Si content of the clay fraction (Si_t), the $\delta^{30}Si_{DCB}$ of the DCB-extracted Si pool can be computed (Table 12.4). The calculated $\delta^{30}Si_{DCB}$ values in SR, MB surface horizons and in DJ horizons were positive (SR) or not in the range of terrestrial reported Si isotopic values (MB, DJ) indicating that Si included in this DCB-extract should be considered very carefully. For the other horizons, we propose a temptative calculation of the Si source for Si in DCB-extract, considering a major control by Fe-oxide.

The studied soils contain various proportions of crystalline and short range ordered (sro) Fe-oxides (Chapter 11), as inferred from Fe_o (sro) and [Fe_d-Fe_o] (crystalline) contents (Suppl. Mat., Table G.3). Si adsorption onto Fe-oxides privileges light Si isotopes (Chapter 10). The fractionation factor $^{30}\varepsilon$ between Si source and Si adsorbed onto synthetic goethite (crystalline) and ferrihydrite (sro) is -1.60‰ and -1.08‰, respectively (Chapter 10). Using the content of crystalline (Fe_d-Fe_o) and sro Fe-oxides (Fe_o), and the corresponding fractionation factor $^{30}\varepsilon$, a mean $^{30}\varepsilon$ for each horizon can be computed (Table 12.4). For small Si isotopic fractionations, $\Delta^{30}Si$ offers a good approximation for $^{30}\varepsilon$, which can be expressed as follows:

$$^{30}\varepsilon \sim \Delta^{30}Si = \delta^{30}Si_{DCB} - \delta^{30}Si_{source} \quad (12.1)$$

where $\delta^{30}Si_{DCB}$ is the signature of the DCB-extracted Si calculated in Table 12.4, and $\delta^{30}Si_{source}$ is the isotopic composition of the unknown Si source. Following Eq. (12.1), the mean source calculated for Si DCB-extracted is -1.08 ± 0.35‰ (Table 12.4). This suggests a large impact of a Si-source enriched in light Si isotopes, e.g. a contribution from the dissolution of primary minerals (-0.38‰) or clay minerals (-1.70 ± 0.79‰ in Mungo).

Biogenic Si contribution to amorphous Si fraction

The ASi fraction consists of biogenic silica (BSi), i.e. plant phytoliths, with a variable contribution of non-crystalline inorganic Si, such as volcanic glass, or sro Si minerals precipitated following oversaturation in soil solution (Chadwick et al., 1987b). In Mungo, the ASi signature at depth is similar to that of fresh pumice (-0.38‰) in DD and DJ, suggesting a major contribution of volcanic glass in ASi (Figure 12.3; Figure 12.5a). In contrast, SR, MB and DJ surface ASi fractions display $\delta^{30}Si$ values in the range of the average $\delta^{30}Si$ balanced for banana plant (+0.33 ± 0.30‰; Chapter 8, Figure 12.5a), whereas MB and DJ ASi

fractions display heavier δ^{30}Si in surface than at depth suggesting the contribution of a heavier Si source in surface horizons (Figure 12.5a). In DD, surface and depth ASi fractions are isotopically close to fresh pumice. Phytoliths were observed in all Mungo surface ASi fractions, but not at depth. From the isotopic signatures of ASi (including phytolith and volcanic glass in surface horizons), the BSi contribution to the SiO_2 content of the ASi fraction can be estimated, assuming δ^{30}Si values for volcanic glass at -0.38‰ (fresh pumice), and for BSi at +0.11‰ (DD), +0.54‰ (DJ) (Chapter 8), and +0.33‰ (mean value between DD and DJ) for SR and MB (Table 12.4). Assuming 100% SiO_2 in BSi and taking into account the measured SiO_2 content in the ASi fraction, the phytolith % in the ASi fraction can be computed. Taking into account the ASi content in the soil, the phytolith % in the soil can be evaluated (Table 12.4). This calculation confirms microscopical observations, i.e. that BSi contribution to total Si content is larger in surface (Ap) than in deep (AC, B) horizons (Table 12.4), and thus supports the surface accumulation of phytoliths. In surface horizons, the estimated BSi contribution is 0, 0.95, 1.72 and 0.82% in DD, SR, MB and DJ, respectively (Table 12.4). The deduced absence of BSi contribution in DD-Ap accords with the dominance of primary minerals, but not with the observation of phytoliths in ASi. This is probably due to the low ASi content of DD (0.6%), strongly diluted in a glass-rich assemblage. A heavier Si source in surface ASi fractions is supported for SR, MB and DJ (Figure 12.5a) by their δ^{30}Si values in the range of the average δ^{30}Si balanced for the whole banana plant (+0.33 ± 0.30‰; Chapter 8).

Isotopic balance in the bulk soil

The δ^{30}Si measured in FEF of DD (-0.41‰) and DJ (-1.41‰) indicate a lighter isotopic signature in the SWvs DJ. Taking into account (i) sand, silt, clay and ASi contents, (ii) the contribution of each fraction to total Si content of the bulk soil, and (iii) the Si isotopic signatures of each fraction, a balanced isotopic signature of the bulk soil can be calculated (Table 12.4). Calculated values for DD (-0.30‰) and DJ (-1.51‰) do not significantly differ from measured values (-0.41‰ and -1.41‰, respectively). The calculated values for SR and MB are -0.43 and -0.76‰, respectively, which are intermediate values between DD and DJ. Two factors have not been taken into account in our calculation: (i) Si contribution from irrigation waters (as an input) and (ii) Si adsorbed onto Fe-oxides. Irrigation waters (mean δ^{30}Si = +1.19‰) would affect all soils similarly. Si adsorption impacts Si isotopic fractionation depending on Fe-oxide content and type (Chapter 10; Chapter 11). However, the

good agreement between measured and calculated δ^{30}Si values suggests that these two potential contributions exert a minor impact on the Si isotopic balance of bulk soils.

12.4.3 Plant impact on silicon cycle in soil

Evidence from δ^{30}Si and Ge/Si

Si isotopic signatures of crystalline clays (see section 12.4.2) in DD, SR and MB are heavier in surface horizons than at depth ($\Delta^{30}Si_{surf\text{-}depth}$ =+0.38 ± 0.04‰), but they did not significantly differ between surface and depth in DJ (Figure 12.5a). In Mt Cameroon, the Si isotopic signature of clay fractions is similar in surface and deep horizons in MO, EK and MU (Table 12.2). These differences might indicate different Si sources for the formation of secondary clays in surface and deep horizons. DD-, SR- and MB-clays are Ge-depleted relative to DJ-clays (Figure 12.5b). Moreover, DD-, SR- and MB-clays are Ge-depleted in surface horizons compared to depth, supporting a different Si source for secondary weathering products in surface compared to depth, as highlighted by δ^{30}Si values (Figure 12.5a). As BSi (phytoliths) was observed in DD, SR, MB and DJ surface horizons (Suppl. Mat., Figure G.5), but not at depth, our data support that BSi is a source for Si sequestration in clay-sized constituents in surface horizons, as previously reported for clay formation (Michalopoulos and Aller, 2004; Michalopoulos et al., 2000). This BSi source likely does not occur in DJ and Mt Cameroon soils, in which clay signatures are very close to that of kaolinite (δ^{30}Si = -2.2‰, Ziegler et al. (2005b); Ge/Si = 5.9μmol/mol, Kurtz et al. (2002)). Surface horizons of Mt Cameroon soils are deeper (Ap2 below 5cm) than in Mungo (Ap 0-5cm), hence diluting BSi pool. The very close signature of surface and deep horizons in DJ should be related to the high clay and Fe-oxide contents, compared to BSi content. Secondary weathering products are well known to be Ge-enriched (Kurtz et al., 2002; Murnane and Stallard, 1990) whereas minor Ge sequestration by Fe-oxides has been reported (Scribner et al., 2006). Consequently, BSi contribution would be hardly detected in soils enriched in clay and Fe-oxide.

Estimation of silicon input from biomass to soils

Soils under study developed from basaltic ash and pumice deposits aged from early Quaternary. Clay formation was gradual over time, while BSi input from banana is about fifty years old. However, the formation of clay minerals from biogenic Si could be very rapid (<1yr) (Michalopoulos

and Aller, 2004). As bananas are Si-accumulating plants (Henriet et al., 2006), a high rate of phytolith restitution to the soil is expected since leaf and pseudostem residues return to soil every 6-9 months, at each harvesting time. An estimation of BSi input to soil since the beginning of banana cropping can be computed, and would represent the maximum potential Si input from banana plant to the soil. Assuming a 25 t yr^{-1} crop yield with a density of 2100 banana plants ha^{-1}, the total dry matter production of a banana crop is estimated to 14 t ha^{-1} yr^{-1} from which ∼10 t dry matter of residues are left in the field (Twyford and Walmsley, 1973). The mean Si concentration in mature banana plant can be calculated from the Si content in each plant part (Suppl. Mat., Table G.4) and corresponding biomass (Martin-Prével and Montagut, 1966). It ranges between 2.7 and 5.7 g $Si.kg^{-1}$ dry matter. So the Si immobilization of a banana crop would range from 27 to 57 kg Si ha^{-1} yr^{-1}. This is in the same range than Si input from equatorial rainforest (41 kg Si ha^{-1} yr^{-1}; Lucas et al. (1993)). At harvesting time, the banana mineralomass is restituted to the soil and provides from 57 to 38 kg Si ha^{-1} yr^{-1} from PDvs (Vitric Andosol) to SWvs

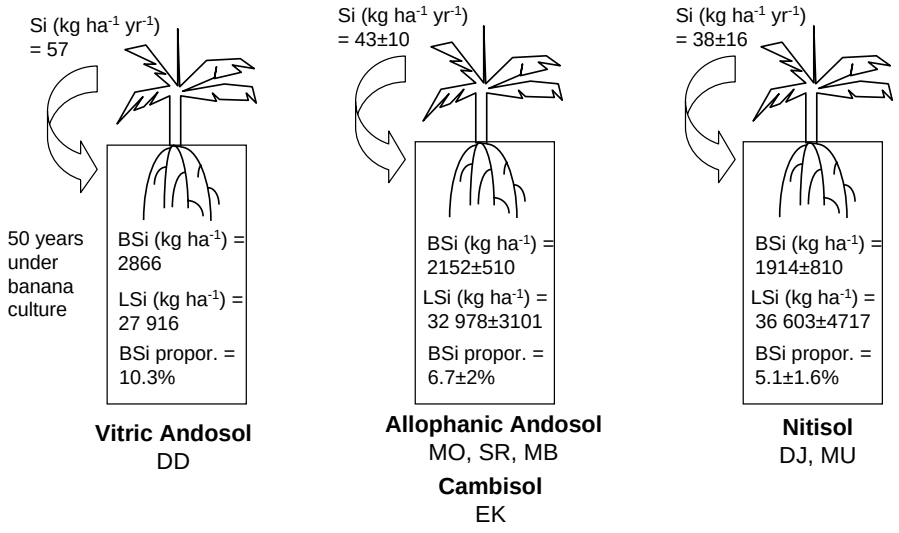

Figure 12.6: Plant input (biogenic Si, BSi) to the soil compared to lithogenic Si pool (LSi) during 50 years of banana culture, and proportion (BSi/LSi) for the Vitric Andosol, Allophanic Andosol, Cambisol and Nitisol (ISSS, 1998). The LSi pool in soils was calculated using the bulk density of surface horizons (Delvaux, 1988) and the total Si content of soil (Suppl.Mat., Table G.1).

(Nitisol) (Figure 12.6). Summing up during the 50 years of banana cropping would give a total BSi input ranging from 2866 to 1915 kg ha^{-1} from Vitric Andosol to Nitisol, respectively. Compared to the 27916 to 36603 kg ha^{-1} range of lithogenic Si (LSi) in soil, BSi would account for 10.3% in the Vitric Andosol, which is significantly larger than in the Allophanic Andosol and Cambisol (6.7%) and Nitisol (5.1%) (Figure 12.6). This conclusion is in excellent agreement with the direct control of weatherable primary minerals on the building-up of the BSi pool in the soil-plant system, as recently demonstrated in a similar weathering sequence of volcanic ash soils (Henriet, 2008). Here, the large BSi input and the apparent low contribution of BSi to total Si in the Vitric Andosol (DD) (Table 12.4) would mean that BSi is quickly dissolved and recycled in the Vitric Andosol. This might explain the heavier Si isotopic signature of clays in the surface horizons of this Andosol (DD, Figure 12.5a). Besides, this confirms the importance of Si biological pumping and restitution by plants (Lucas, 2001). We therefore suggest that this BSi pool can represent an additional Si source for Si sequestration in secondary weathering products through clay formation and Si adsorption onto Fe-oxides.

12.4.4 Implications on the biogeochemical Si cycle

Our data provide answers to the questions raised in the Introduction. (1) Si isotopic signatures of bulk soils (FEF) are strongly determined by the relative proportions of primary and secondary minerals, and hence weathering stage. (2) The BSi pool readily contributes to Si sequestration in clay-sized fractions through clay formation and Si-adsorption on Fe-oxide in surface horizons of the least weathered soils because weatherable lithogenic minerals strongly influence the building up of BSi. (3) δ^{30}Si and Ge/Si are pertinent proxies to follow weathering and clay formation in soils, and to estimate the input of BSi into the soil-plant system under study, i.e. involving a Si accumulating plant. Our data confirm that weathering and soil development lead to build up a pool of stable secondary weathering products enriched in light Si isotopes and Ge (Kurtz et al., 2002; Ziegler et al., 2005b), and thereby impact dissolved phases exported to rivers and oceans, enriched in heavy Si isotopes (Alleman et al., 2005; De La Rocha et al., 2000; Ding et al., 2004; Georg et al., 2006a 2007c) and depleted in Ge (Derry et al., 2005). These soil processes can be monitored in other environments. Similar approaches can thus be followed, taking into account biomass production and Si uptake rate by plants, e.g. in equatorial rainforest (Alexandre et al., 1997) or temperate forest (Gérard et al., 2008). Here, intensive

banana cropping restitutes significant BSi to soil, and thus significantly impacts the Si recycling in surface horizons. Our data further support BSi as a source for clay formation in PDvs surface horizons, clays being isotopically heavier (δ^{30}Si) and Ge-depleted. The impact of weathering on the DSi isotopic signal depends on lithology and weathering intensity (Georg et al., 2007c), but Si biocycling will impact all soil environments supporting Si-accumulating plants. These processes would impact the riverine isotopic signal to ocean, as continental runoff water contributes to more than 80% of the input to the marine Si budget (Tréguer et al., 1995).

12.5 Conclusions

Both δ^{30}Si and Ge/Si proxies trace the increasing weathering of volcanic ash soils under study, leading to isotopically negative and Ge-enriched clays. Si isotopic compositions of soil fractions allow evaluating the quartz contribution from saharian dust in soil surface horizons, and the BSi contribution in these horizons. δ^{30}Si and Ge/Si signatures of clays support the presence of a BSi source available for Si sequestration in clays of PDvs surface horizons. Bulk soil signatures were mainly determined by the proportions of primary and secondary minerals, and were poorly impacted by dissolved Si. We conclude that δ^{30}Si and Ge/Si are highly pertinent proxies to study the Si soil-plant cycle, and to identify the major processes impacting the bulk soil isotopic signature. Weathering and Si biocycling would impact the exported isotopic signal.